PERGAMON

International Journal of Rock Mechanics & Mining Sciences 38 (2001) 369–378

International Journal of
Rock Mechanics
and Mining Sciences

www.elsevier.com/locate/ijrmms

A three-dimensional slope stability analysis method using the upper bound theorem
Part I: theory and methods

Zuyu Chen[a,*], Xiaogang Wang[b], C. Haberfield[c], Jian-Hua Yin[d], Yujie Wang[d]

[a] *Department of Hydraulic Engineering, China Institute of Water Resources and Hydropower Research, Tsinghua University, 20, West Chegongzhuang Rd., PO Box 366, Beijing 100044, China*

[b] *China Institute of Water Resources and Hydropower Research, PO Box 366, Beijing, China*

[c] *Department of Civil Engineering, PO Box 60, 3800, Australia*

[d] *Department of Civil and Structural Engineering, The Hong Kong Polytechnic University, Hong Kong*

Accepted 8 January 2001

Abstract

A three-dimensional (3D) slope stability analysis method, based on its two-dimensional approaches proposed by Donald and Chen (Can. Geotech. J. 34 (1997) 853.) is presented in this paper. It starts from establishing a compatible velocity field and obtains the factor of safety by the energy and work balance equation. Optimisation is followed to approach the critical failure mode that offers the minimum factor of safety. The method is demonstrated to be identical to Sarma's limit equilibrium method (1979) that employs inclined slices, if it is extended to the 3D area. However, it has been established on a sound theoretical background supported by the upper bound theorem of plasticity. Test problems have demonstrated its feasibility. A feature of the method is its very simple way to obtain the factor of safety without complicated 3D force equilibrium evaluations. Limited assumptions are involved in this method and their applicability has been justified.

Keywords: Slope stability analysis; Three-dimensional analysis; Upper bound theorem; Limit analysis

1. Introduction

Stability analyses of slopes are routinely performed by two-dimensional (2D) limit equilibrium methods. For rock slopes, conventional methods developed for soil slopes, e.g. Bishop's simplified method recommended by Hoek and Bray [1], are often adopted. However, other methods, e.g. Sarma [2] which employs slices with inclined interfaces to simulate structural discontinuities, have been highly commended [3]. Unfortunately, most of these analyses are limited to two dimensions, which cannot properly model the true three-dimensional (3D) characteristics of a landslide. A practical 3D slope stability analysis method and the related computer programs are therefore urgently required [4,5].

There are a large number of publications that deal with 3D slope stability analysis. In general, these methods can be classified into two categories.

(1) *The limit equilibrium approaches*: Duncan [6] reviewed the main aspects of 24 publications dealing with limit equilibrium approaches. The failure mass is divided into a number of columns with vertical interfaces and the conditions for static equilibrium are used to find the factor of safety. Hungr [7], Hungr et al. [8], Chen and Chameau [9] and Lam and Fredlund [10] extended Bishop's simplified, Spencer's and Morgenstern and Price's methods from two to three dimensions, respectively. However, only limited reports on the application of these methods have been documented. Stark and Eid [11] reviewed three commercially available computer programs in their attempts to analyse several landslide case histories and concluded that "the factor of safety is poorly estimated by using commercially available software because of limitations in describing geometry, material properties and/or the analytical methods".

*Corresponding author. Tel.: 86-10-685-148-24; fax: 86-10-684-383-17.

E-mail address: chenzy@tsinghua.edu.cn (Z. Chen).

1365-1609/01/$ - see front matter
PII: S1365-1609(01)00012-0

In general, the methods of columns with vertical interfaces suffer the following limitations:

- A large number of assumptions have to be introduced to render the problem statically determinate. Lam and Fredlund [10] balanced the number of equations that can be established from physical and mechanical requirements to the number of unknowns involved in these equations. They found that, for a failure mass divided into n rows and m columns (refer to Fig. 1), a total of $8mn$ assumptions are required.
- The method is further hampered by complicated 3D vector analysis that generally involves a set of non-linear simultaneous equations. Iteration is necessary to obtain a solution unless further simplifications are introduced.
- Since the method as applied to three dimensions is in its infancy, no attempt has yet been published to find a critical 3D slip surface of a generalised shape.

(2) *The upper bound approaches*: The basic principles of the upper bound theory of plasticity as applied to 2D geomechanical problems are well documented [12]. Publications dealing with this subject in three dimensions is also available [13,14]. Most of the work is based on analytical approaches in which the failure mass is divided into several blocks with simplified slip surface shapes such as straight or logarithmic lines. The often complex geometry of the surface of the slope is usually simplified to a plane described by two straight lines. The material is assumed to be homogeneous and ground water conditions are either ignored or over-simplified. These simplifications have limited the application of these methods to practical problems.

Recently, Donald and Chen [15] proposed a 2D slope stability analysis method that is based on the upper bound theorem but arrives at a solution numerically. The failure mass is divided into slices with inclined interfaces. They demonstrated that this method is equivalent to Sarma's method of non-vertical slices and therefore is particularly applicable to rock slopes. However, unlike Sarma's original work that employed force equilibrium, they started the calculation by establishing a compatible velocity field and obtained the factor of safety by the energy-work balance equation. The subsequent automatic search for the critical failure modelled to success in finding accurate solutions for a number of closed-form solutions provided by Sokolovski [16].

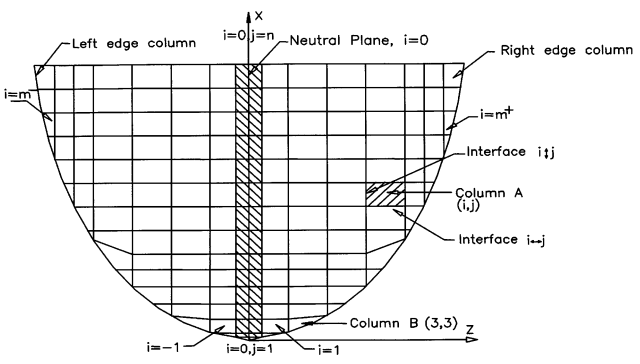

Fig. 1. A plan view of the discretisation pattern for a 3D failure mass.

The method described in this paper is an extension of Donald and Chen's 2D approach. The failure mass is divided into a number of prisms with inclined interfaces. It uses the upper-bound theory and therefore avoids introducing a large number of assumptions. In three dimensions, the solution for the factor of safety still remains a scalar manipulation of energy-force balance without the need for complicated non-linear 3D force equilibrium equations. Optimisation routines are followed to find the critical failure mode.

PART I of this paper describes the principles and methods of this approach, while PART II gives the numerical procedures and their applications and extensions to a number of typical 3D rock slope stability problems such as those concerned with arch dam abutments and tunnel portals.

2. Theoretical background

2.1. The upper bound method

The statement of the upper bound theorem, as it applies to soil mechanics, is described in Chen [12]. Its application to slope stability analysis is discussed by Donald and Chen [15].

For a slope that is at limit state, the material within the sliding surface, represented as Ω^*, is assumed to be plastic everywhere and therefore at yield. Under these conditions, the upper bound theorem states that among all possible external loads applied to a kinematically admissible plastic zone Ω^*, the external load T that brings about failure on a failure mode Ω, can be approached by minimising T^* as determined from the following work-energy balance equation.

$$\int_{\Omega^*} \sigma_{ij}^* \cdot \dot{\varepsilon}_{ij}^* \mathrm{d}v + \int_{\Gamma^*} \mathrm{d}D_s^* = \boldsymbol{W}\boldsymbol{V}^* + \boldsymbol{T}^*\boldsymbol{V}^*, \tag{1}$$

where $\boldsymbol{V}^*$ is the rate of plastic displacement, generally referred to as the plastic velocity. $\boldsymbol{W}$ is the body force corresponding to the plastic zone. The left-hand side of Eq. (1) represents the rate of internal energy dissipation within the failure mass and along the slip surface.

The 3D energy approach described herein approximates the failure mass by a series of prisms having rectangular inclined side faces (Figs. 1 and 2).[1] For this

[1] The term prisms has been used rather than the more usual term of columns to avoid confusion with the rows and columns of a matrix.

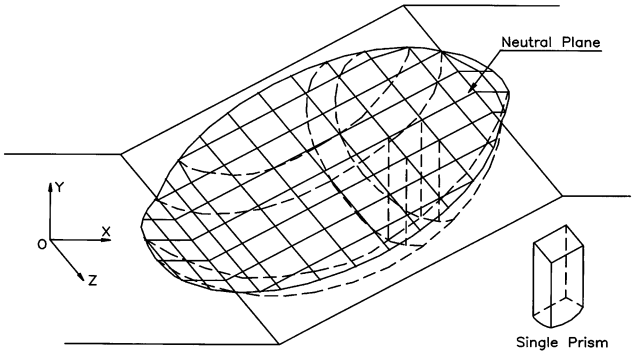

Fig. 2. An isometric view of the discretisation pattern for a 3D failure mass.

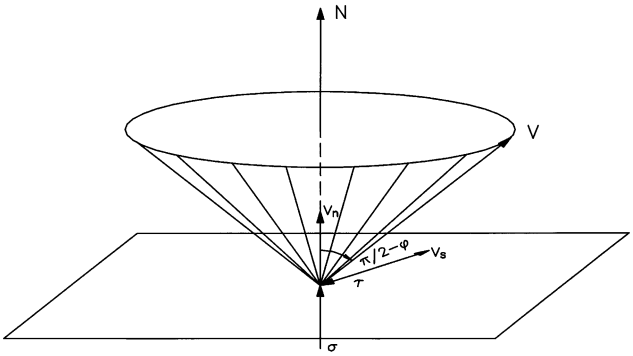

Fig. 3. The orientations of the plastic vectors determined based on the associated flow law.

form of discretisation, Eq. (1) may be approximated in the form of a summation.

$$\sum D^*_{i\leftrightarrow j} + \sum D^*_{i\updownarrow j} + \sum D^*_{i,j} = \boldsymbol{W}\boldsymbol{V}^* + \boldsymbol{T}^*\boldsymbol{V}^*, \qquad (2)$$

where the symbol $\updownarrow$ is used to represent the interfaces between two adjacent columns and $\leftrightarrow$, between two adjacent rows of prisms (refer to Fig. 1). The three terms in the left-hand side of the equation approximate the energy dissipation on the row-to-row and column-to-column interfaces and on the slip surface, respectively.

For a soil or rock slope that is subjected to an external load T^o, the upper bound theorem states that the loading factor η, defined as

$$\eta = \frac{T^o - T^*}{T^o} \qquad (3)$$

should approach its minimum in order to bring the structure to failure. Other alternatives include the coefficient of critical horizontal acceleration of the body force applied on the failure mass, as suggested by Sarma [2] and discussed by Donald and Chen [15]. The main advantage of using these approaches is that η can be determined in a straightforward way from Eq. (2) without the need for iteration.

The stability of a slope is generally assessed by determining the factor (of safety), F, by which the available shear strength parameters c' and ϕ' need to be reduced to bring the structure to a limit state of equilibrium. The reduced parameters c'_e and ϕ'_e can therefore be defined by

$$c'_e = c'/F, \qquad (4)$$

$$\tan\phi'_e = \tan\phi'_e/F. \qquad (5)$$

The upper bound method therefore requires that the minimum value of F related to a critical failure mechanism and determined from Eq. (6) be found.

$$\sum D^*_{i\leftrightarrow j,\,e} + \sum D^*_{i\updownarrow j,\,e} + \sum D^*_{i,j,\,e} = \boldsymbol{W}\boldsymbol{V}^* + \boldsymbol{T}^o\boldsymbol{V}^*. \qquad (6)$$

The three terms with subscript 'e' on the left-hand side of Eq. (6) are determined on the basis of the reduced strength parameters defined by Eqs. (4) and (5). For the remainder of this paper, the subscript 'e' is attached to any variable that has been calculated using these reduced strength parameters.

2.2. Plastic velocity and energy dissipation

The upper bound solution described in this paper is obtained by applying Eq. (1) to the assumed plastic velocity developed on a Mohr–Coulomb yield surface, which is given by the following equation:

$$f(\tau,\,\sigma) = \tau - c'_e - (\sigma - u)\tan\phi'_e = 0, \qquad (7)$$

where τ and σ' are the shear and normal total stresses on the failure plane, respectively, and u is the pore pressure. For an associative flow rule, the normal velocity V_n and tangential velocity V_s obey the following relationship:

$$\frac{V_\mathrm{n}}{V_\mathrm{s}} = \frac{\partial f/\partial\sigma}{\partial f/\partial\tau} = -\tan\phi'_e. \qquad (8)$$

This implies that for a Mohr–Coulomb material, the plastic velocity is inclined at an angle of ϕ'_e to the failure plane. From a 3D point of view, the vector $\boldsymbol{V}$ lies within an inverted cone of revolution (Fig. 3) defined by an axis normal to the failure plane and subtending an included angle of $(\pi/2-\phi'_e)$; i.e.

$$\boldsymbol{\Phi}(\boldsymbol{V},\,\boldsymbol{N}) = \cos\left(\frac{\pi}{2} - \phi'_e\right) = \sin\phi'_e, \qquad (9)$$

where $\boldsymbol{N}$ represents the vector of the normal to the failure plane.

The Mohr–Coulomb failure criterion can also be expressed in terms of the major and minor principal stresses, respectively, σ'_1 and σ'_3,

$$\tfrac{1}{2}(\sigma'_1 - \sigma'_3)\cos\phi'_e = c'_e - [\tfrac{1}{2}(\sigma'_1 + \sigma'_3) + \tfrac{1}{2}(\sigma'_1 - \sigma'_3)\sin\phi'_e]\tan\phi'_e. \qquad (10)$$

As the Mohr–Coulomb failure criterion does not include the intermediate principal stress, the plastic strain increment will only exist in the plane constituted by the major and minor principal stresses. In other words, the normal stress, shear stress, and the plastic velocity

vector all lie in the same plane (Fig. 3). This important conclusion has enabled the calculation of the internal energy dissipation in an identical manner to the 2D approach. The work done by the internal total stress on a unit area of the failure surface can be determined without the knowledge of the internal stresses, which are generally unknown anyway.

$$\begin{aligned} \mathrm{d}D &= \tau V_{\mathrm{s}} + \sigma V_{\mathrm{n}} = (\tau \cos \phi'_e + \sigma \sin \phi'_e)V \\ &= (c \cos \phi'_e - u \sin \phi'_e)V. \end{aligned} \tag{11}$$

In Eq. (11), the term $c \cos \phi_e V$ is the internal energy dissipation developed by the effective stresses and, $u \sin \phi_e V$ is the work done by pore water pressure but treated as a term of negative energy dissipation for convenience.

2.3. The relationship between the upper bound and force equilibrium approaches

It has been shown [15] that solving Eqs. (2) or (6) is equivalent to the conventional slope stability analysis procedures that employ force equilibrium approaches. Michalowski [13] showed that in some cases both approaches gave the same results. However, he argued that from a theoretical point of view, they should not be regarded as equivalent. For better understanding of the framework to this 3D stability analysis method, it is advantageous to investigate further herein through a two-wedge example, as shown in Fig. 4. For this problem, if we assume that Mohr–Coulomb failure criterion applied on both the bases and the interface, we can solve the factor of safety in either of the following two ways.

Method 1*, the energy approach*: In the upper bound method, the plastic velocities applied to the left and right wedges, $\boldsymbol{V}_{\mathrm{l}}$ and $\boldsymbol{V}_{\mathrm{r}}$, respectively, and the relative velocity of the left wedge with respect to the right wedge, $\boldsymbol{V}_j$, need to be determined. By definition we have

$$\boldsymbol{V}_j = \boldsymbol{V}_{\mathrm{l}} - \boldsymbol{V}_{\mathrm{r}}. \tag{12}$$

Since $\boldsymbol{V}_{\mathrm{l}}$, $\boldsymbol{V}_{\mathrm{r}}$ and $\boldsymbol{V}_j$ are all inclined at angle ϕ'_e to their respective failure surfaces, the magnitude of $\boldsymbol{V}_{\mathrm{r}}$ and $\boldsymbol{V}_j$ can be determined as a function of $\boldsymbol{V}_{\mathrm{l}}$ [15],

$$V_{\mathrm{r}} = V_{\mathrm{l}} \frac{\sin(\theta_{\mathrm{l}} - \theta_j)}{\sin(\theta_{\mathrm{r}} - \theta_j)}, \tag{13}$$

$$V_j = V_{\mathrm{l}} \frac{\sin(\theta_{\mathrm{r}} - \theta_{\mathrm{l}})}{\sin(\theta_{\mathrm{r}} - \theta_j)}, \tag{14}$$

where θ is the angle of the velocity vector measured from the positive x-axis. Neglecting the pore pressure terms in this two-wedge problem, Eq. (6) becomes

$$\begin{aligned} &A_{\mathrm{l}}\, c'_{\mathrm{l},e} \cos \phi'_{\mathrm{l},e}\, V_{\mathrm{l}} + A_{\mathrm{r}}\, c'_{\mathrm{r},e} \cos \phi'_{\mathrm{r},e}\, V_{\mathrm{r}} \\ &\quad + A_j\, c'_{j,e} \cos \phi'_{j,e}\, V_j = W_{\mathrm{l}}\, V_{\mathrm{l}} \cos \rho_{\mathrm{l}} + W_{\mathrm{r}}\, V_{\mathrm{r}} \cos \rho_{\mathrm{r}} \end{aligned} \tag{15}$$

where ρ is the angle between the weight vector and the velocity and A is the area of the failure surface on which $\boldsymbol{V}$ applies. By virtue of Eqs. (13) and (14), V_{r} and V_j can be expressed as a linear function of V_{l}, and therefore can be deleted as it is contained in all terms of Eq. (15). Eq. (15) then involves only one unknown, the factor of safety F, which is implicitly included in c'_eandϕ'_e and can be readily solved by iteration.

Method 2*, the force equilibrium approach*: If we assume that the Mohr–Coulomb criterion applies on both the slip surface and the inclined interfaces between the wedges, the forces applied on a failure plane can be divided into two components:

(1) The cohesion force $\boldsymbol{C}_e$ developed by c'_e on the area A, and
(2) The friction force $\boldsymbol{P}_e$ defined as the resultant of the normal force $\boldsymbol{N}$ and its contribution to shear resistance on the failure surface, which has a magnitude of $N \tan \phi'_e$.

$\boldsymbol{P}_e$ is inclined at angle ϕ'_e to the normal to the failure surface. Therefore, only its magnitude P_e remains unknown, see Fig. 4.

Considering force equilibrium for the left and right wedges, respectively, leads to

$$\boldsymbol{W}_{\mathrm{l}} + \boldsymbol{P}_{\mathrm{l},e} + \boldsymbol{P}_{j,e} + \boldsymbol{C}_{\mathrm{l},e} + \boldsymbol{C}_{j,e} = 0 \tag{16}$$

and

$$\boldsymbol{W}_{\mathrm{r}} + \boldsymbol{P}_{\mathrm{r},e} + \boldsymbol{P}'_{j,e} + \boldsymbol{C}_{\mathrm{r},e} + \boldsymbol{C}_{j,e} = 0, \tag{17}$$

where $\boldsymbol{P}_{j,e}$ is the inter-wedge force applied to the left wedge by the right wedge. $\boldsymbol{P}'_{j,e}$ is the reaction of $\boldsymbol{P}_{j,e}$, and is exerted by the left wedge on the right wedge. $\boldsymbol{C}_{j,e}$ is the cohesion force developed on the interface.

$$\boldsymbol{P}_{j,e} = -\boldsymbol{P}'_{j,e}. \tag{18}$$

Resolving into the x and y directions, Eqs. (16) and (17) yield four equations which permit the determination of the four unknowns, $P_{\mathrm{l},e}$, $P_{\mathrm{r},e}$, $P_{j,e}$ and F. The problem is therefore, statically determinate and the solution for the factor of safety is unique.

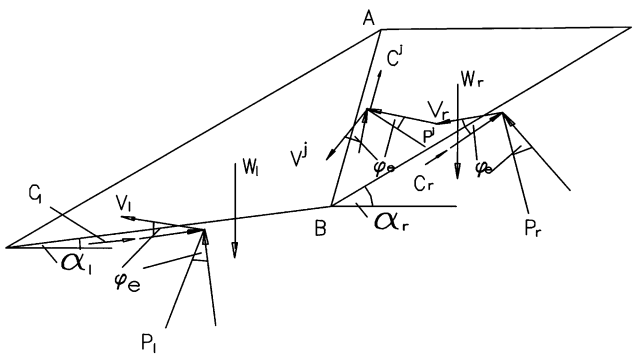

Fig. 4. A two-wedge example used to explain the equivalence between the force equilibrium and energy approaches.

However, the principle of virtual work provides a more efficient way of solving Eqs. (16) and (17) for F. To employ this method, virtual displacements $\boldsymbol{V}_{\mathrm{l}}, \boldsymbol{V}_{\mathrm{r}}, \boldsymbol{V}_j$ (Fig. 4) inclined at angle ϕ'_e to their respective shear surfaces are assigned. $\boldsymbol{P}_{\mathrm{l}}, \boldsymbol{P}_{\mathrm{r}}$ and $\boldsymbol{P}_j$ are unknown perpendiculars to $\boldsymbol{V}_{\mathrm{l}}, \boldsymbol{V}_{\mathrm{r}}$ and $\boldsymbol{V}_j$, respectively, and do zero work on them. Multiplying Eqs. (16) and (17) by $\boldsymbol{V}_{\mathrm{l}}$ and $\boldsymbol{V}_{\mathrm{r}}$, respectively, and summing leads to the following work-energy balance equation,

$$\boldsymbol{W}_{\mathrm{l}}\boldsymbol{V}_{\mathrm{l}} + \boldsymbol{W}_{\mathrm{r}}\boldsymbol{V}_{\mathrm{r}} + \boldsymbol{C}_{\mathrm{l},e}\,\boldsymbol{V}_{\mathrm{l}} + \boldsymbol{C}_{\mathrm{r},e}\,\boldsymbol{V}_{\mathrm{r}} + \boldsymbol{C}_{j,e}\,\boldsymbol{V}_j = 0. \quad (19)$$

Eq. (19) is identical to Eq. (15). Sarma's method obtains the factor of safety by solving Eqs. (16) and (17), leaving Eq. (19) to be satisfied automatically, while the upper bound approach finds the solution by employing Eqs. (19) and (16), leaving Eq. (17) to be satisfied automatically. If the factor of safety is the primary concern, then implementation of the upper bound method ceases with the solution of Eq. (15).

The above demonstration shows that the conventional limit equilibrium method of inclined slices can be solved in a more efficient way. Extensions of this approach to 3D analysis will bring vital advantages, as the solution still remains as a single equation similar to Eq. (15) provided that the velocity field can be determined.

3. The velocity field in three dimensions

3.1. The co-ordinate system and discretisation pattern

In a similar manner to the 2D limit equilibrium method, the failure mass is divided into a number of prisms with inclined inter-prism sides.

The assumption is made that inside the failure mass there exists a plane, called the neutral plane, on which there is no lateral movement relative to the main direction of sliding. For a symmetric failure mass, the neutral plane is the vertical plane of symmetry that strikes in a direction representing the main direction of sliding. In some applications (e.g. the wedge failure analysis) the neutral plane is the central plane within the failure mass, on which the prisms move in a parallel direction. The co-ordinate system $ox-oy$ is established in this plane; oy is opposite to gravity, ox is perpendicular to oy and opposite to the direction of sliding and oz is established based on the right-hand rule. In the neutral plane, the normal component of the velocity at any point in the z direction is assumed to be zero or a constant.

Each prism is approximated by a hexahedron as shown in Fig. 5. The base ABCD forms a part of the slip surface. EFGH forms a part of the slope surface. ABFE and DCGH are front and rear surfaces, respectively, and are represented by the symbol $\leftrightarrow$ and called the

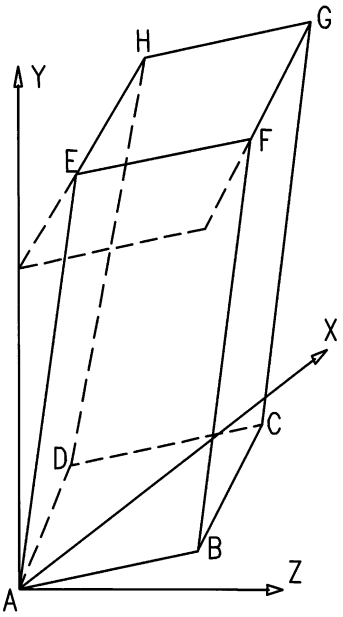

Fig. 5. A hexahedral prism.

'row-to-row' interfaces. They are perpendicular to the plane xoy. The left and right sides, ADHE and BCGF, respectively, are perpendicular to the plane yoz, and are represented by the symbol $\updownarrow$ and called the 'column-to-column' interfaces. Rock slopes in general contain one or several sets of sub-vertical discontinuities that provide a realistic discretisation pattern for these inclined interfaces. If these discontinuities do not exist, such as in a soil slope, the inclinations of these interfaces will be changed in a subsequent calculation until the minimum factor of safety is obtained.

In plan, there are n rows of prisms in the ox direction. In the positive and negative oz directions, there are m^+ and m^- columns of prisms respectively (Fig. 1). The first column of prisms in the ox direction have plane xoy as their axis are numbered $i = 0$. The prisms of the second column in the positive oz direction are numbered $i = 1$. In the positive oz direction $i = 0, 1, \ldots, m^+$, while in the negative oz direction, $i = 0, -1, \ldots, m^-$. Henceforth, all the following derivations are concerned with prisms that are in the positive oz direction. The derivations equally apply to those in the negative oz direction. The prisms are numbered from 1 to n in the ox direction in the neutral plane. A prism located in the ith column in the oz direction and jth row in the ox direction is therefore numbered i, j.

3.2. Calculating the velocity field

The prism numbered i, j has a velocity designated by $\boldsymbol{V}_{i,j}$. The relative velocity of prism i, j with respect to column $i-1, j$ (i.e, that on the column-to-column interface) is designated $\boldsymbol{V}_{i\updownarrow j}$. $\boldsymbol{V}_{i\leftrightarrow j}$ then represents the

relative velocity of prism i, j with respect to prism $i, j-1$. Refer to Fig. 1.

The velocity of a prism relative to its immediate neighbours is calculated on the basis of satisfying the flow law and displacement compatibility. There are three different cases to be considered:

Case 1. *The velocity field of the prisms at the neutral plane*: Calculating the velocities of the column series $i=0$, i.e., those of the prisms at the plane *xoy*, is equivalent to the method used in the two-dimensional energy approach. In this case, the inclination angle between $\boldsymbol{V}_{i,j}$ and the *xoy* plane for all prisms are zero or a constant. Given $\boldsymbol{V}_{0,j-1}$, $\boldsymbol{V}_{0,j}$ and $\boldsymbol{V}_{0\leftrightarrow j}$ can be found using Eqs. (13) and (14).

Case 2. *The velocity field of the prisms remote from the edges of the failure mass*: The velocity $\boldsymbol{V}_{i,j}$ of prism i, j is determined based on the velocities of their left and lower neighbouring columns $\boldsymbol{V}_{i-1,j}$ and $\boldsymbol{V}_{i,j-1}$ (refer to Fig. 6(a)).

It is a requirement that

$$\Phi(\boldsymbol{V}_{i,j}, \boldsymbol{N}_{i,j}) = \sin\phi'_{i,j}, \tag{20}$$

$$\Phi(\boldsymbol{V}_{i\updownarrow j}, \boldsymbol{N}_{i\updownarrow j}) = \sin\phi'_{i\updownarrow j}, \tag{21}$$

$$\Phi(\boldsymbol{V}_{i\mapsto j}, \boldsymbol{N}_{i\mapsto j}) = \sin\phi'_{i\mapsto j}, \tag{22}$$

where $\Phi(\boldsymbol{V}, \boldsymbol{N})$ can be determined by

$$\Phi(\boldsymbol{V}, \boldsymbol{N}) = \frac{X\cdot L + Y\cdot M + Z\cdot N}{\sqrt{X^2+Y^2+Z^2}\cdot\sqrt{L^2+M^2+N^2}} \tag{23}$$

in which X, Y, and Z are components of $\boldsymbol{V}$, and L, M, and N, the direction cosines of the normal to the failure plane.

Since $\boldsymbol{V}_{i-1,j}$ and $\boldsymbol{V}_{i,j-1}$ are known, Eqs. (20)–(22) are sufficient to determine the three components of $\boldsymbol{V}_{i,j}$ with the definitions

$$\boldsymbol{V}_{i\leftrightarrow j} = \boldsymbol{V}_{i,j} - \boldsymbol{V}_{i,j-1} \tag{24}$$

$$\boldsymbol{V}_{i\updownarrow j} = \boldsymbol{V}_{i,j} - \boldsymbol{V}_{i-1,j}. \tag{25}$$

Case 3. *The velocity of a column located at the edge of the failure mass*: Consider the velocity of the first prism of a prism series, which is numbered i, k (prism A in Fig. 6(b)). It can be referred to as an edge prism. It has a left neighbouring prism $i-1, k$ but no lower neighbouring prism. $\boldsymbol{V}_{i,k}$ can only be determined based on the known velocity $\boldsymbol{V}_{i-1,k}$. In this case, the two available Eqs. (20) and (21) are not sufficient to determine $\boldsymbol{V}_{i,k}$ as there are three unknown components. One additional condition therefore needs to be introduced to determine the velocity of the lower first prism of a column series.

Assume that the magnitude of $\boldsymbol{V}_{i,k}$ of prism i can be related to that of prism $\boldsymbol{V}_{i-1,k}$, by a factor ξ_i, that is,

$$|V_{i,k}| = \xi_i |V_{i-1,k}|. \tag{26}$$

With this additional assumption, it is now possible to determine the velocity of the edge prism of each series. The values of ξ_1, ξ_2, ξ_3, ..., can be determined using a rigorous procedure that will be explained in Section 4.2. It is also shown that setting $\xi_i = 1$ leads to a solution with sufficient accuracy.

The computation procedure for the determination of the whole velocity field includes the following steps:

(1) Set the velocity of the first prism in the neutral plane, i.e., $\boldsymbol{V}_{0,1}$, to be unity. $\boldsymbol{V}_{0,2}$ and $\boldsymbol{V}_{0\leftrightarrow 2}$ can be determined based on the procedure of Case 1. Successive integration will allow the determination of $\boldsymbol{V}_{0,j}$ and $\boldsymbol{V}_{0\leftrightarrow j}, j=2,\ldots,n$.
(2) Calculate, $\boldsymbol{V}_{1,k}$, the velocity of the edge prism numbered 1, k from $\boldsymbol{V}_{0,k}$ based on the procedures for Case 3.
(3) Start with $\boldsymbol{V}_{1,k}$, calculate $\boldsymbol{V}_{1,j}, \boldsymbol{V}_{1\updownarrow j}$ and $\boldsymbol{V}_{1\leftrightarrow j}$ $(j=k, k+1,\ldots,)$, for the prism series $i=1$, based on the procedures of Case 2 by successive integration.
(4) Calculate the velocities of the column series numbered $i=2,\ldots,m^+$ by the same procedures as outlined in steps (2) and (3).
(5) Calculate the velocities of the column series to the left of the neutral plane, i.e., $i=-1,\ldots,m^-$ in a similar manner to steps (2)–(4).

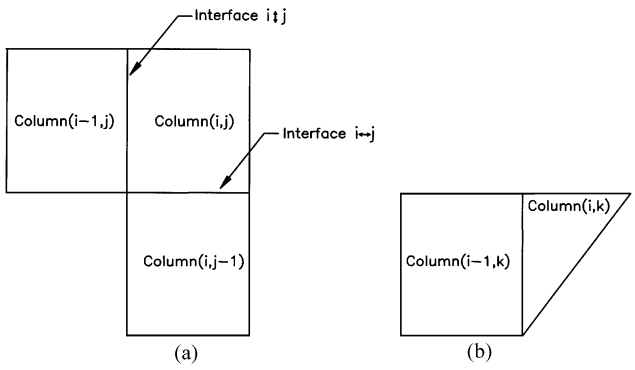

Fig. 6. Calculation of the velocity of a prism. (a) Case 2, and (b) Case 3.

4. The energy method

4.1. Determination of F and η

Once the velocity field is known, the energy dissipation on the slip surface and interfaces involved in Eq. (6) can be readily determined by Eq. (11). Subsequently, T^*, or the loading factor η defined by Eq. (2), can be obtained.

Iteration is necessary when using Eq. (6) to solve for F, which is implicitly involved in Eqs. (4) and (5). As with the 2D case, iteration is performed by assuming a series of values for F and calculating their associated

loading factors η. The Newton–Raphson technique is recommended to find the value of F that gives a value of $\eta = 0$. Convergence is generally not of concern since the procedure involves only one variable.

4.2. Discussion on the assumptions

The method described previously involved several assumptions. Firstly, it employs the associative flow law. Very few soil or rock materials display associative behaviour during loading. However they do exhibit dilatancy during failure, and more or less offer a plastic deformation inclined at an angle of ϕ' to the failure plane at this particular limiting equilibrium state. Therefore, its adoption in the upper bound method where loading only during failure is concerned can be justified on the basis that it considerably simplifies the solution process without a significant loss in accuracy.

Furthermore, even though the material does not exhibit plastic deformation behaviour similar to what has been assumed, the demonstrated equivalence between the force equilibrium and energy methods ensures that implementing Eq. (6) at least offers a solution that satisfies force equilibrium conditions.

The second assumptions are those involved in determining the velocity field, i.e., a neutral plane and a set of ξ_i in the calculation for the velocities of the edge prisms.

It has been found that these assumptions can be avoided if the numerical procedure described previously proceeds to calculate the forces applied on the slip surface and the interfaces [17]. This has been made possible since, as is stated in Section 2.2, the shear force on the failure surface should lie on the plane defined by the normal of the failure surface and the velocity. Therefore, once the procedure for calculating the factor of safety is completed, the direction of the shear forces are known, resulting in a considerable reduction in the number of unknowns in the force equilibrium equations. It has been found that the number of unbalanced force equilibrium equations just matches the number of assumptions needed to define the directions of velocities on the neutral plane and the values of ξ_i. An iterative procedure will permit the determination of these assumed values [17]. However, the numerical procedures can be very complicated. This is not generally acceptable in the area of slope stability analysis where rapid solutions are required. As a result, slope stability analyses have a long history of employing various simplified methods to solve practical problems successfully. From a practical point of view, it is sufficient to adopt the simplified approach of a neutral plane and the assumption for ξ_i. Some justification for this simplified approach can be obtained by applying the method to practical problems,

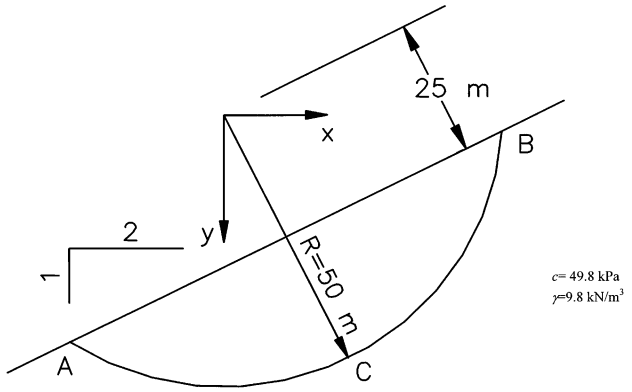

Fig. 7. Example 1—spherical slip surface in a purely cohesive soil.

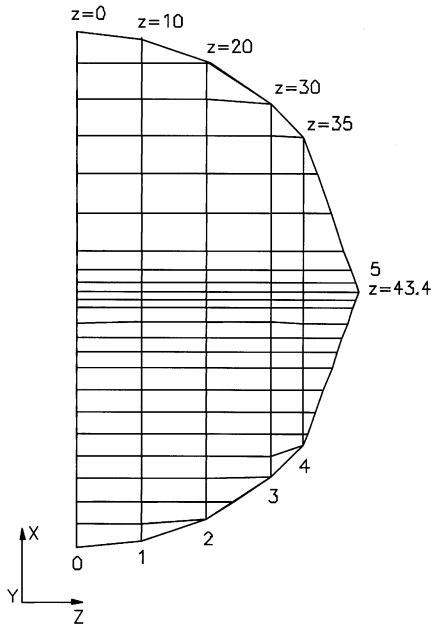

Fig. 8. The plan view of the discretisation pattern for Example 1.

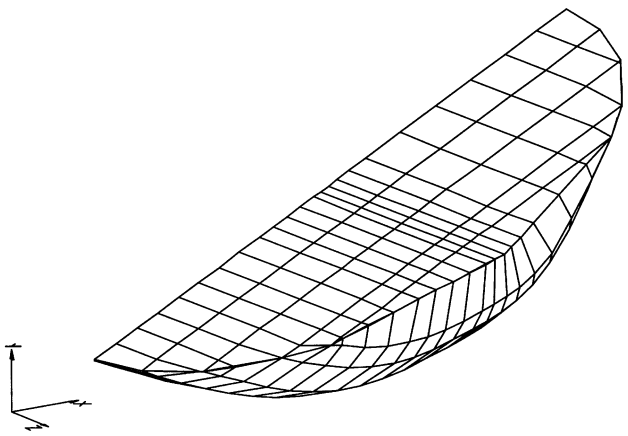

Fig. 9. An isometric view of the discretisation pattern for Example 1.

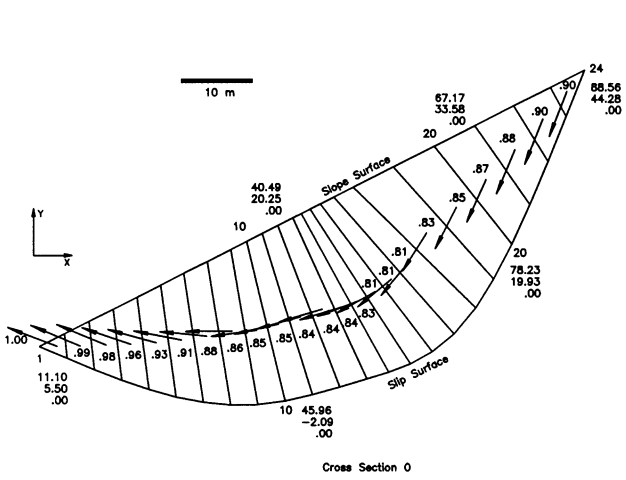

(a) 100%

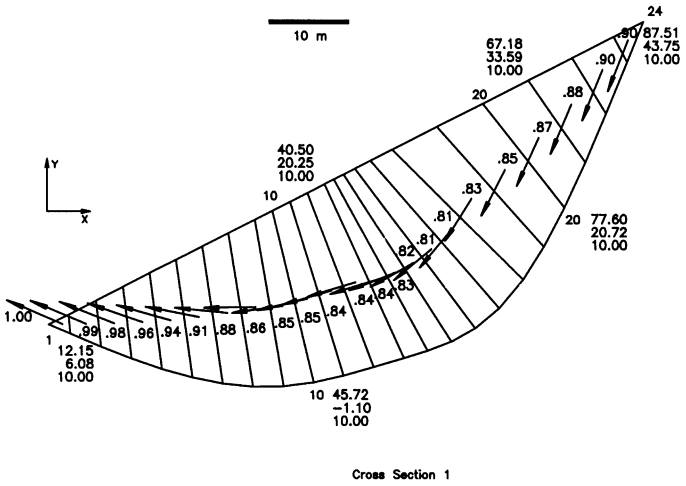

(b) 110%

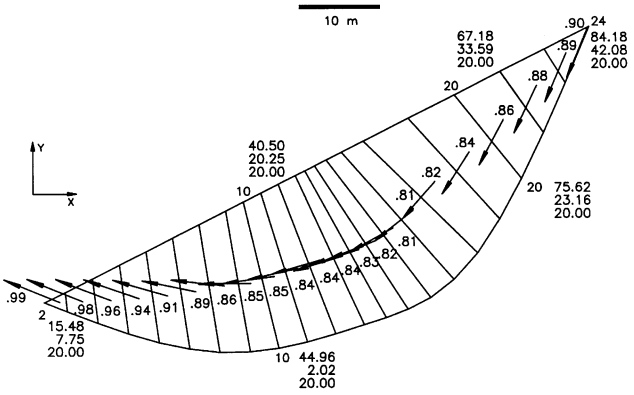

(c) 110%

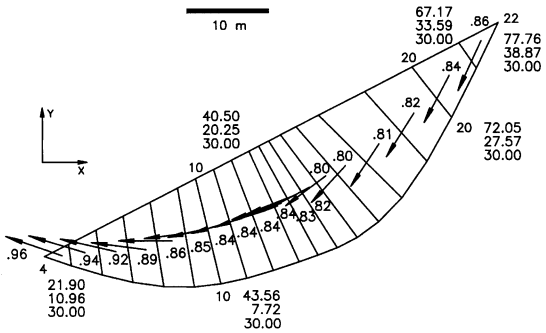

(d) 110%

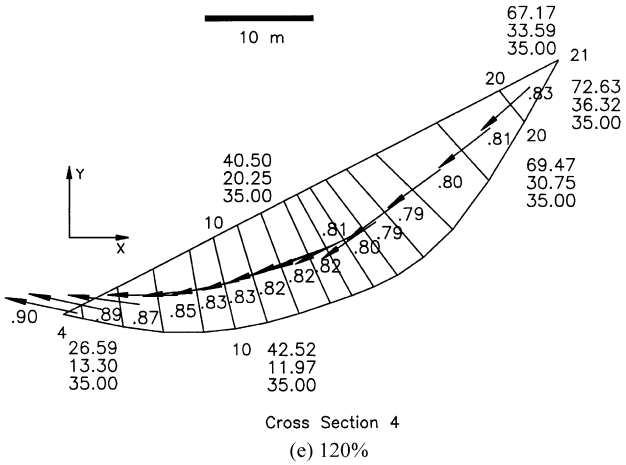

(e) 120%

Fig. 10. (a–e). The velocity field for each cross section.

and studying the effect of variations in the assumed parameters on the solution. It is also theoretically acceptable to try several different locations for neutral planes and different values for ξ_i. The one associated with the minimum factor of safety will most likely represent the acceptable solution.

5. Test problems

A computer program EMU-3D has been coded for 3D slope stability analysis. Two test examples that have been documented in the literature were performed to investigate the feasibility of this method.

Example 1. *A spherical failure surface in a purely cohesive soil*: Fig. 7 shows the simple problem of a uniform slope and a spherical slip surface. This problem has been extensively addressed in the literature [7,10]. Assuming that the forces applied to the sphere are all parallel to the $x-y$ plane and by enforcing moment equilibrium about the z-axis, it is possible to obtain a factor of safety of 1.402. Although this is only one of many possible solutions that satisfy equilibrium conditions, it is widely referred to as a 'closed-form' solution.

Since the failure surface has a symmetric shape, only half of the failure mass was considered during analysis. Initially, the failure surface was divided into 24 row-to-row and 5 column-to-column interfaces as shown in Figs. 8 and 9, and ξ_i was taken to be unity for all edge prisms. This case led to the solution $F = 1.504$. Fig. 10 shows the velocities of the prisms at various cross sections. Fig. 10 investigates the sensitiveness of the assumed values of ξ_i introduced in Eq. (26). It has been found that the values of ξ_i are indeed not sensitive to the solution. As the variation in magnitudes of the velocities on the neutral plane are only of the order of 0.90 (Fig. 11(a)), there is no need for investigation of ξ_i beyond the range shown in Fig. 11(a). Most importantly, Fig. 11(a) clearly shows that taking ξ_i to be unity gives the minimum values of F. Therefore in the subsequent calculations ξ_i was always taken to be unity.

This solution was improved by inclining the row-to-row interfaces and searching for the critical inclination mode using the optimisation methods described in PART II of this paper. The resulting minimum factor of safety was $F_m = 1.422$.

Refinement of this solution was sought by inclining the column-to-column interfaces. The coefficient of inclination is defined as

$$\omega_i = \frac{z^i_{n,u} - z^{i-1}_u}{z^i_u - z^{i-1}_u}, \tag{27}$$

where z^i_u and $z^i_{n,u}$ refer to the z values on the slope surface of the original vertical and subsequent inclined interfaces, respectively, while the superscript i refers to the number of the interface (Fig. 12). The present study only includes a constant value of ω for all columns. It has been found that the factors of safety associated with $\omega = 1.1$, or 0.9 were greater than that associated with $\omega = 1.0$. Therefore, the final solution obtained was $F_m = 1.422$. Table 1 summarises the factors of safety obtained at various steps, compared with those documented in the literature.

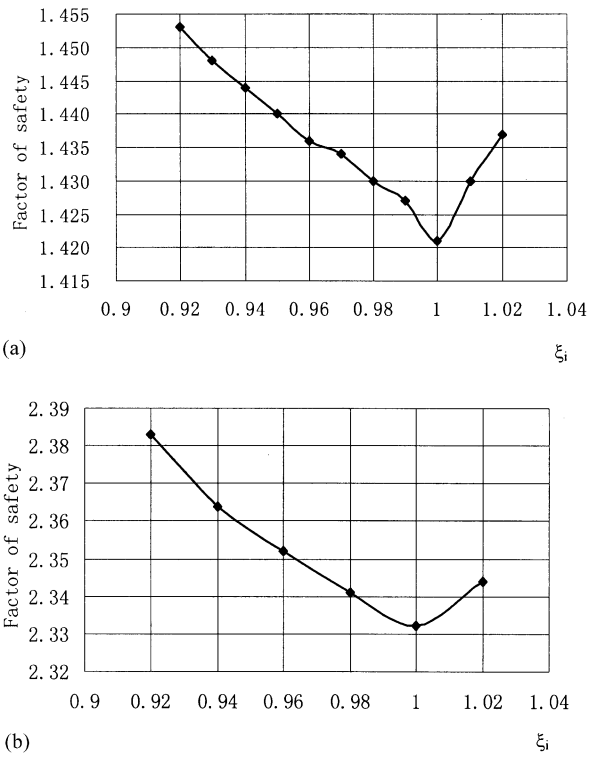

Fig. 11. Variations of F with ξ_i, (a) Example 1, (b) Example 2.

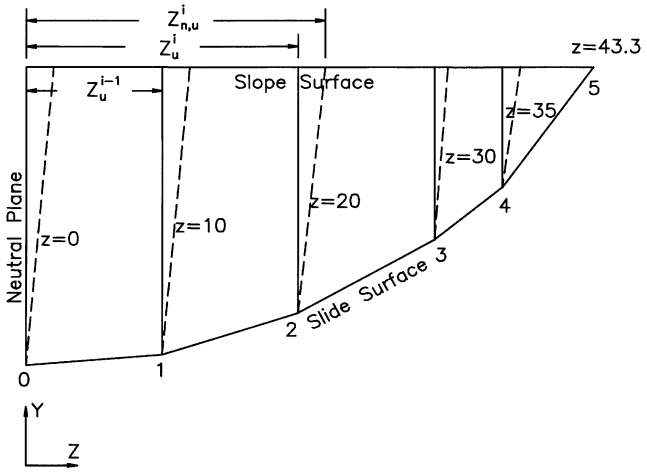

Fig. 12. Inclinations of the cross sections.

Table 1
Solutions obtained by various methods

Method	F
'Closed-form'	1.402
CLARA (Hungr et al. [8])	1.422
3D-slope 1200	1.386
Lam and Fredlund [10] 500	1.402
EMU-3D	
$\omega = 1.0$	1.422
$\omega = 1.1$	1.480

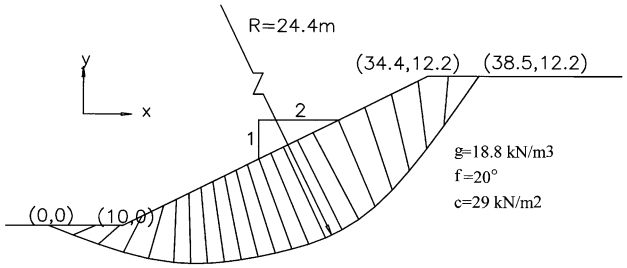

Fig. 13. Example 2—Elliptical slip surface in a cohesive-frictional material.

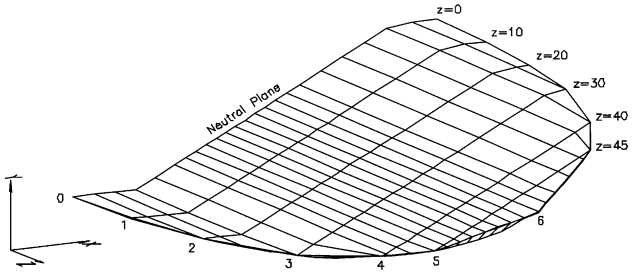

Fig. 14. An isometric view of the discretisation pattern for Example 2.

Example 2. *A partly elliptical failure surface in a cohesive-frictional material*: Fig. 13 shows another example that has also been referred to in [18]. The homogeneous slope material has both c' and ϕ' as depicted in the figure. The slip surface is created by a circle at the central plane and a series of elliptic lines extending in z direction, as shown in Fig. 14. Similar to Test Problem 1, the failure mass on the right side of the neutral plane is divided into 6 vertical column-to-column planes at a spacing of 10 m. The initial input failure mode gave a factor of safety of 2.332. Fig. 11(b) shows the relationship between F and ξ_i which again showed minor variations in factors of safety associated with different values of ξ_i and a minimum value of F at $\xi_i = 1$. The optimisation process eventually led to the interface inclinations shown in Fig. 13 with a minimum factor of safety of $F = 2.262$. This can be compared to the value of $F = 2.122$ obtained by Zhang [18] using the limit equilibrium method.

6. Concluding remarks

The upper bound plasticity method has distinct advantages over other methods as it is mathematically rigorous, virtually free of assumptions, and is numerically simple and stable. On extension to three dimensions, these advantages to a large extent still remain. This paper demonstrates that extending the traditional 2D method of slices to a 3D method of prisms is possible. The velocity field can be determined in a simple way using a limited number of assumptions. The final solution has been shown to be relatively insensitive to these assumptions.

Like many of the conventional 3D slope stability analysis methods that are extensions of simplified 2D approaches, the method presented in this paper is actually an extension of Sarma's 2D method of non-vertical slices. However, the solution is obtained from a much more efficient energy-work balance equation. The solution is supported by the Theory of Plasticity if the calculated velocity field represents a real plastic deformation mechanism. The inclined interfaces between prisms offer a unique advantage of modelling rock slopes with sub-vertical discontinuities, as is illustrated in PART II of this paper.

References

[1] Hoek E, Bray JW. Rock slope engineering. The Institute of Mining and Metallurgy, 1977.
[2] Sarma KS. Stability analysis of embankments and slopes. J Geotech Am Soc Civ Eng 1979;105(12):1511–24.
[3] Hoek E. General two-dimensional slope stability analysis. In: Brown ET, editor. Analytical and computational methods in engineering rock mechanics. London: Allen & Unwin, 1987. p. 95–128.
[4] Seed RB, Mitchell JK, Seed HB. Kettlemen hills waste landfill slope failure, II: stability analysis. J Geotech Eng ASCE 1990;116(4):669–90.
[5] Morgenstern NR. The evaluation of slope stability—a 25 year perspective. In: stability and performance of slopes and embankments. ASCE Geotechincal Special Publications, 1992. p. 1–26.
[6] Duncan JM. State of the art: limit equilibrium and finite element analysis of slopes. J Geotech Eng ASCE 1996;122(7):577–96.
[7] Hungr O. An extension of Bishops simplified method of slope stability analysis to three dimension. Geotechnique 1987;37:113–7.
[8] Hungr O, Salgado FM, Byrne PM. Evaluation of a three-dimensional method of slope stability analysis. Can Geotech J 1989;26:679–86.
[9] Chen R, Chameau JL. Three-dimensional limit equilibrium analysis of slopes. Geotechnique 1983;33:31–40.
[10] Lam L, Fredlund DG. A general limit-equilibrium model for three-dimensional slope stability analysis. Can Geotech J 1993;30:905–19.
[11] Stark TD, Eid HT. Performance of three-dimensional slope stability analysis method in Practice. J Geotech Eng ASCE 1998;124:1049–60.
[12] Chen WF. Limit analysis and soil plasticity. New York: Elsevier Scientific Publishing Co., 1975.
[13] Michalowski RL. Three-dimensional analysis: of locally loaded slopes. Geotechnique 1980;39:27–38.
[14] Lin M, Drescher A. Limit load in steady 3-D plastic flow around obstacles. In: Pietruszczak S, Pande GN, editors. Numerical models in geomechanics, NUMOG III. Amsterdam: Elsevier, 1989. p. 297–304.
[15] Donald I, Chen ZY. Slope stability analysis by the upper bound approach: fundamentals and methods. Can Geotech J 1997;34:853–62.
[16] Sokolovski VV. Statics of soil media. (Translated by Jones DH and Scholfield AN) Butterworth, London, 1960.
[17] Chen ZY. Study on the abutment stability of Xiaowan Arch Dam. Internal Report, China Institute of Water Resources and Hydropower Research, No. 96-221-03, 1999 [in Chinese].
[18] Zhang X. Three-dimensional stability analysis of concave slopes in plan view. ASCE J Geotech Eng 1988;114:658–71.